ACS OMEGA

http://pubs.acs.org/journal/acsodf

Article

An Efficient Catalyst Derived from Carboxylated Lignin-Anchored Iron Nanoparticle Compounds for Carbon Monoxide Hydrogenation Application

Hengfei Qin,* Yan Li, Ruoyu Dong, Jiafeng Yuan, Yue Zhou, Yaxin Hu, Hailang Jia, Jirong Bai, Jie Gong, Jinlong Jiang, and Quanfa Zhou*

Cite This: *ACS Omega* 2021, 6, 16592−16599

Read Online

ACCESS | Metrics & More | Article Recommendations

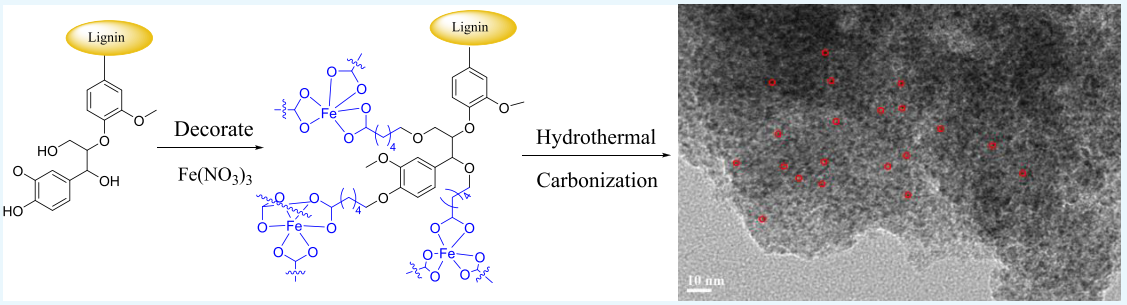

ABSTRACT: Catalytic activity and target product selectivity are strongly correlated to the size, crystallographic phase, and morphology of nanoparticles. In this study, waste lignin from paper pulp industry is employed as the carbon source, which is modified with carboxyl groups at the molecular level to facilitate anchoring of metals, and a new type of carbon-based catalyst was obtained after carbonization. As a result, the size of the metal particles is effectively controlled by the chelation between $-COO^-$ and Fe^{3+}. Furthermore, Fe/CM-CL with a particle size of 1.5−2.5 nm shows excellent catalytic performance, the conversion of carbon monoxide reaches 82.3%, and the selectivity of methane reaches 73.2%.

1. INTRODUCTION

Fischer−Tropsch synthesis (FTS) is a green and sustainable route that can directly convert synthesis gas (H_2 + CO) into lower olefins (C_2-C_4) or fuel oil under the action of a catalyst.[1−4] It is of considerable significance to solve the problem of environmental pollution caused by traditional petroleum-processing technologies. The commercial FTS catalyst is supported by Ru, Fe, Co, and other metals on SiO_2, TiO_2, Al_2O_3, and other oxides or molecular sieves and carbon materials.[5−13] In recent years, metals or metal oxides supported on carbon materials (M_xO_y/CMs) have aroused the interest of many researchers.[8,14−18] Relevant reports show that M_xO_y/CMs have the following advantages as catalysts for FTS: (1) carbon materials can regulate the interaction between the active metal and the support; (2) carbon materials can change the acid−base center of the catalyst; (3) carbon materials are beneficial to the reduction of metals and the improvement of the dispersion of metals on the surface of the support. These advantages show an excellent prospect for the design and applications of carbon materials in the FTS catalyst. However, there are still some short plates. For example, is it possible to control the size of metal nanoparticles using carbon materials? At present, it has been reported that the size and dispersion of metal particles have a significant influence on the catalytic performance. Hensen et al.[19] reported that Fe nanoparticles smaller than 7−9 nm show higher CH_4 selectivity compared with larger particles. De Jong et al.[20,21] mentioned that methane is the dominant product when Fe nanoparticles are less than 7 nm, and the selectivity of CH_4 reaches 64% when the size of Fe nanoparticles is 2.2 nm (2FeCNF). Therefore, it is a challenge for the FTS catalyst to adjust the size of metal particles through carbon supports.

Carbon sources are one of the main factors affecting the fine regulation of the M_xO_y/CM morphology and particle size. At present, the most common carbon sources for the preparation of M_xO_y/CMs are ethanol,[22] methane,[23] butane,[24] benzene,[25] and so forth. However, there are some shortcomings in the preparation of M_xO_y/CMs from the abovementioned conventional carbon sources. First, most of these carbon sources are

Received: April 11, 2021
Accepted: June 4, 2021
Published: June 18, 2021

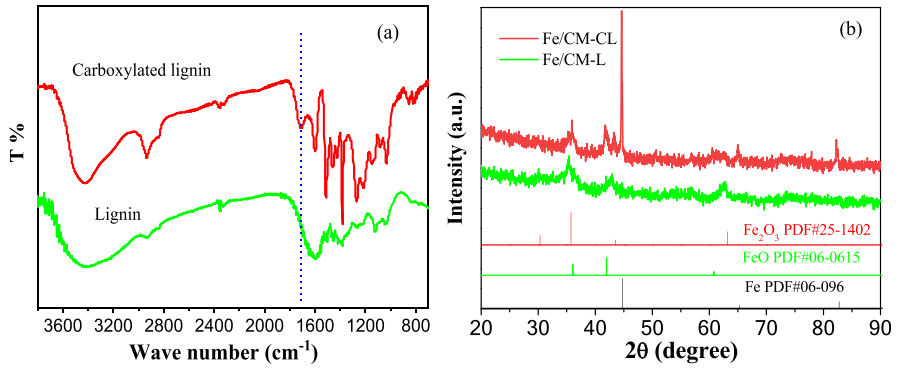

Figure 1. (a) FT-IR spectra of lignin and carboxylated lignin and (b) XRD spectra of Fe/CM-CL and Fe/CM-L.

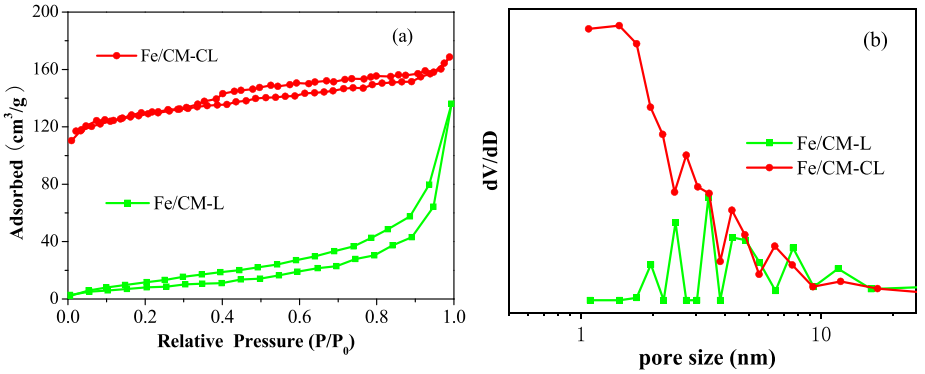

Figure 2. (a) N_2 adsorption−desorption isotherms and (b) corresponding pore size distribution curves of Fe/CM-CL and Fe/CM-L catalysts.

fossil fuels, which are nonrenewable resources. Second, the surface of these carbon sources cannot be modified, and it is difficult to form a coordination structure with metal ions, which affects the excellent control of the morphology of metals and carbon materials. Therefore, it is necessary to find an ideal carbon source whose surface molecular structure is controllable and renewable.

Lignin is second only to cellulose in plants and is regenerated at a rate of two hundred billion tons per year. The paper and pulp industry not only separates about 120 million tons of cellulose from plants each year but also obtains about 50 million tons of lignin byproducts, so it has rich sources and low prices.[26−30] Furthermore, lignin is a natural biopolymer composed of repeating units of *p*-hydroxyphenyl, guaiacyl, and syringyl. There are many aldehyde and hydroxyl groups in the structure, and these functional groups have higher activity, which is conducive to surface modification.[31,32] For example, spherical lignin with a uniform size can be obtained by modifying the surface functional groups, and highly dispersed microspheres can be obtained by changing the hydrophilic and hydrophobic properties of the surface groups of lignin.[33,34] Grafting amino groups on the surface of lignin can improve the antibacterial properties of lignin.[35] Therefore, lignin has the potential of surface group structure regulation and being renewed, which is an ideal carbon source for the preparation of M_xO_y/CM catalysts. In this study, the surface modification method is proposed to introduce carboxyl groups on the surface of lignin, promote the coordination of metal ions and lignin under hydrothermal conditions, construct metal lignin complexes, and obtain a small-size iron catalyst with a uniform size after carbonization.

2. RESULTS AND DISCUSSION

As observed from the Fourier-transform infrared (FT-IR) spectra of lignin and carboxylated lignin (CL) (Figure 1a), both CL and raw lignin exhibited a broad feature around 3400 cm^{-1} and 2940 cm^{-1}, which can be ascribed to the O-H stretching vibrations and asymmetrical stretching vibrations of $-CH_2-$ and $-CH_3-$, respectively. These bands indicate that the skeleton structure of lignin remains intact in the reaction.[37,38] However, there are apparent differences between the carboxylate lignin and raw lignin. The intensities of FT-IR peaks corresponding to C-O stretch (1150 cm^{-1}, H units), C-O stretch (1263 cm^{-1}, G units), and syringyl C-O stretch (1360 cm^{-1}) are significantly stronger than those of the original lignin.[39,40] Furthermore, the strong peak around 1718 cm^{-1} indicated a band of carboxyl stretching vibrations,[41] indicating that modified lignin contains carboxyl functional groups.

The powder X-ray diffraction (PXRD) patterns of Fe/CM-CL are shown in Figure 1b. Fe/CM-CL is composed mainly of metal iron and ferrous oxide. The characteristic peaks that appeared in the positions of 44.6°, 65.0°, and 82.3° are indexed to the (110), (200) and (211) reflections for metal iron (JCPDS Card No. 06−0696), respectively. In addition, the three peaks at around 36.0°, 41.9°, and 60.7° correspond to the (111), (200), and (220) reflections for ferrous oxide (JCPDS Card No.06−0615). For comparison, the XRD pattern of a Fe/CM-L material prepared using the unmodified original lignin is also included in Figure 1b. The peaks at around 30.2°, 35.6°, 43.4°, and 63.0° can be indexed as (206), (119) (0012), and (4012) diffraction planes of Fe_2O_3 (JCPDS Card No. 25−1402), respectively. This phenomenon shows that the combination of iron and carbon is weak in the carbonization

https://doi.org/10.1021/acsomega.1c01935
ACS Omega 2021, 6, 16592−16599

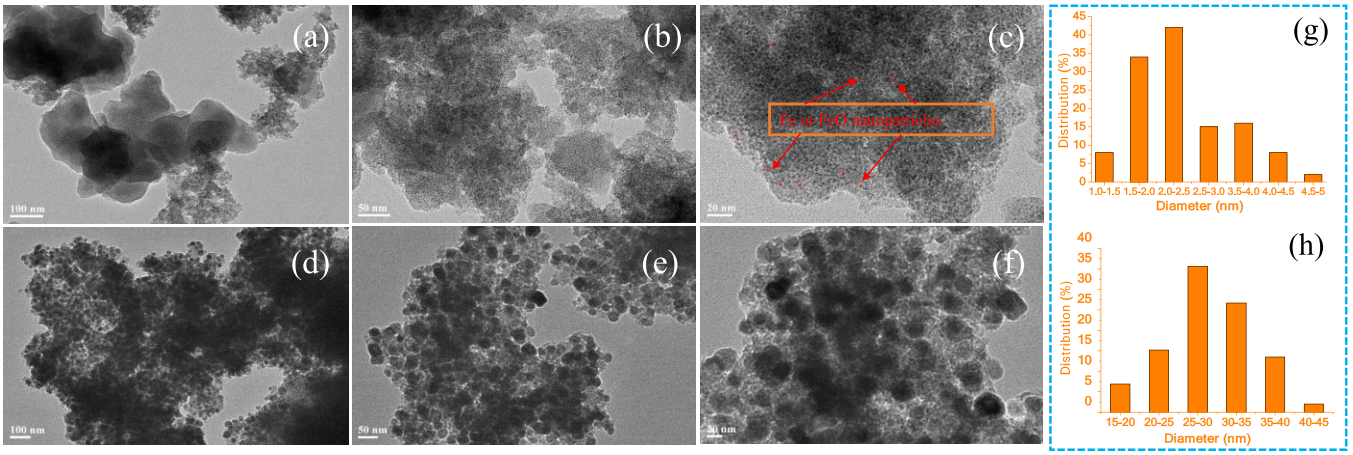

Figure 3. TEM images and particle size distributions of catalysts (a–c, g) Fe/CM-CL and (d, e, h) Fe/CM-L.

process when introducing a carboxyl group of fat chains, which is beneficial to the reduction of iron oxide to metallic iron.

The N_2 adsorption–desorption isotherms and corresponding pore size distribution curves of Fe/CM-CL and Fe/CM-L are shown in Figure 2. In Figure 2a, Fe/CM-CL shows a strong uptake at relative pressure P/P_0 = 0.01–0.1 and a H4-type hysteresis loop at the relative pressure P/P_0 = 0.35–0.85, indicating the existence of micropore and mesoporous structures, which can be ascribed to a type-IV (according to the IUPAC classification) isotherm.[42,43] The specific surface areas calculated from the adsorption portion with P/P_0 under 0.3 were 462.5 $m^2 \cdot g^{-1}$ and 79.2 $m^2 \cdot g^{-1}$ for Fe/CM-CL and Fe/CM-L, respectively. The Fe/CM-CL shows a higher surface area than Fe/CM-L, which is beneficial for the adsorption of syngas, thus enhancing the catalytic performance. The pore size distribution curves were calculated from an analysis of the desorption branch of isotherms, as shown in Figure 2b. It can be seen that the pore diameter of the Fe/CM-L is determined to be around 2–15 nm, while the Fe/CM-CL display micropores less than 2 nm and mesopores around 5–8 nm. This change indicates that the carboxyl functional group is a critical parameter to obtain hierarchical porous carbon materials.

Transmission electron microscopy (TEM) images display further information on the textural properties of Fe/CM-CL and Fe/CM-L catalysts, as shown in Figure 3. As shown in Figure 3a-c, the Fe/CM-CL catalyst is composed of dense black iron nanoparticles that are uniformly distributed in the carbon matrix without agglomeration. It can be seen that the agglomerates of iron particles are observed over the Fe/CM-L catalyst, and they display a broad particle size distribution (Figure 3d–f). From Figure 3g,h, it can be seen that the particle size distribution of the Fe/CM-CL catalyst is about 1.5–2.5 nm, which is only one-tenth of the Fe/CM-L (25–35 nm). The reason for this phenomenon may be attributed to the lignin carboxyl functional group, and iron ion can coordinate in the hydrothermal stage, which can effectively restrain the agglomeration and growth of iron nanoparticles.

Field-emission scanning electron microscopy (FE-SEM) in combination with energy-dispersive spectrometry (EDS) mapping images displayed the morphology of the Fe/CM-CL catalyst, as shown in Figure 4. The Fe/CM-CL catalyst was prepared using CL and iron ions through two steps of hydrothermal carbonization, which exhibited a coarse surface and an amorphous structure. Obviously, the Fe nanoparticles

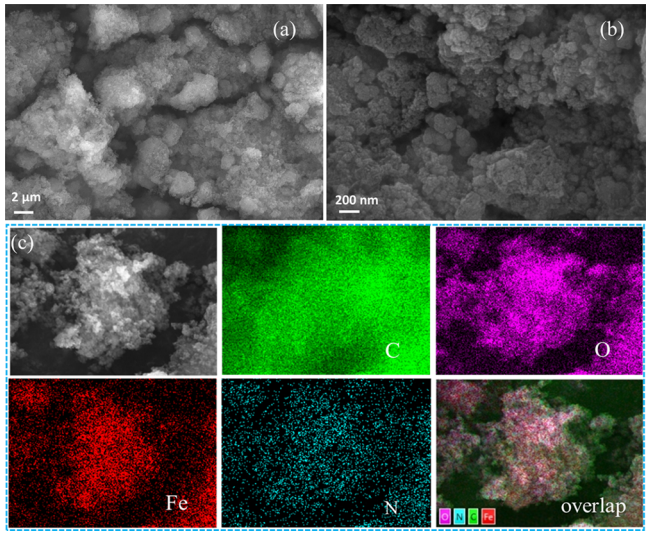

Figure 4. (a), (b) FE-SEM and (c) EDS mapping images of the Fe/CM-CL catalyst.

were uniformly attached to the carbon matrix (Figure 4a,b). C, O, N and Fe atoms are clearly shown in the EDS mapping images (Figure 4c). The C, O, N elements are all originated from lignin and Fe are uniformly distributed in Fe/CM-CL, further confirming the successful growth of iron nanoparticles in carbon matrix.

The presence of different framework elements and the chemical state of the Fe/CM-CL was detected by X-ray photoelectron spectroscopy (XPS). The survey XPS spectrum (Figure 5a) indicates the coexistence of Fe, O, N, and C in the Fe/CM-CL, which agrees well with the FE-SEM elemental mapping results. The fitted high-resolution C 1 s spectrum exhibits three peaks at about 284.6, 285.7, and 288.6 eV, which can be assigned to C–C, C–N, and C=O, respectively.[44] As displayed in Figure 5c, the survey XPS spectrum for N1s can be deconvoluted into four peaks with binding energies 398.3, 399.8, 401.1, and 403.9 eV, which are attributed to pyridinic N, pyrrolic N, graphitic N, and oxidized N, respectively.[45,46] It has been well established that the graphitic N species can promote electron transfer, and pyridinic N plays a significant role in the formation of active sites. Furthermore, XPS measurements reveal the valence state of Fe elements in Fe/CM-CL. The XPS spectrum for Fe 2p (Figure 5d) can be divided into three pairs

https://doi.org/10.1021/acsomega.1c01935
ACS Omega 2021, 6, 16592–16599

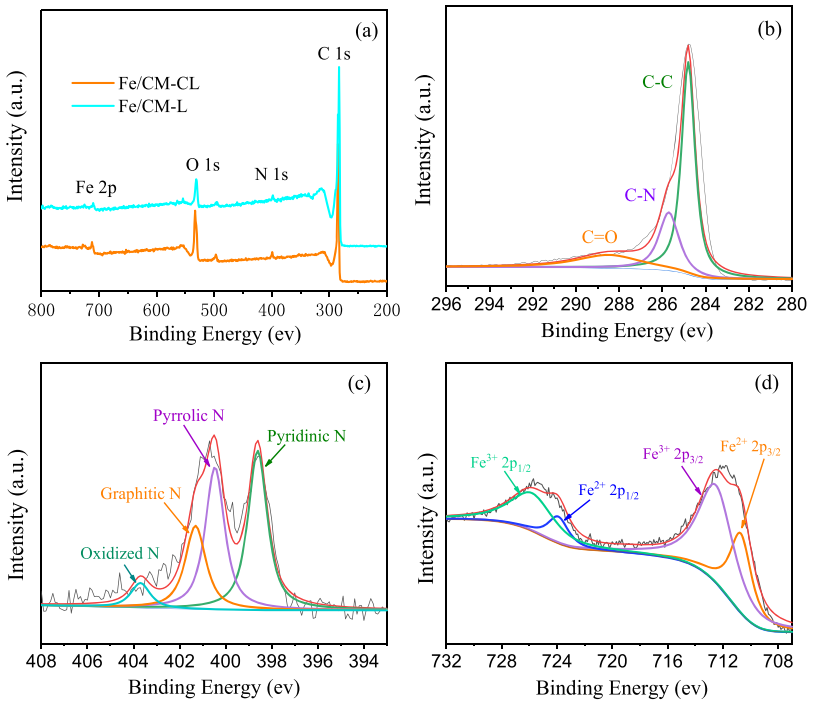

Figure 5. (a) Wide XPS survey spectra of Fe/CM-CL and Fe/CM-CL, (b) high-resolution C 1s spectra of Fe/CM-CL, (c) N 1s spectra of Fe/CM-CL, and (d) Fe 2p spectra of Fe/CM-CL.

Table 1. Comparison of the Catalytic Performance of Catalysts with Different Fe Nanoparticles

					selectivity (%, CO_2-free)					
catalysts	T (°C)	GHSV	particle size (nm)	CO con. (%)	CH_4	$C_2 \sim C_4$ olefins	$C_2 \sim C_4$ paraffins	C_{5+}	CO_2 con. (%)	ref
FeMn/S50	300	5 $gcat^{-1}$·mol^{-1}	13.7	44.0	11.7	43.5	15.5	29.3	34.1	48
2IM	340	360 h^{-1}	2.5	9	34.0	13.0	46.0	2.0	32	20
5FeCNF	350	12,000−24,000 h^{-1}	4.0	10	68.0	19.0	12.0	1.0	-	21
10Fe/hCNC	350	12 L·h-1·$gcat^{-1}$	7.4 ± 3	1.7	27.1	44.4	4.7	23.8	16.5	49
Fe/CM-L	350	8 L·h-1·$gcat^{-1}$	25−30	63.5	28.6	33.6	25.1	12.7	35.9	this work
Fe/CM-CL	350	8 L·h-1·$gcat^{-1}$	1.5−2	82.3	73.2	15.9	9.6	1.3	37.5	this work
Fe/CM-CL	350	12 $L{\cdot}h^{-1}{\cdot}gcat^{-1}$	1.5−2	52.1	60.9	18.8	13.8	6.5	31.4	this work
Fe/CM-CL	340	8 L·h-1·gcat-1	1.5−2	65.9	64.9	15.1	12.2	7.8	34.8	this work

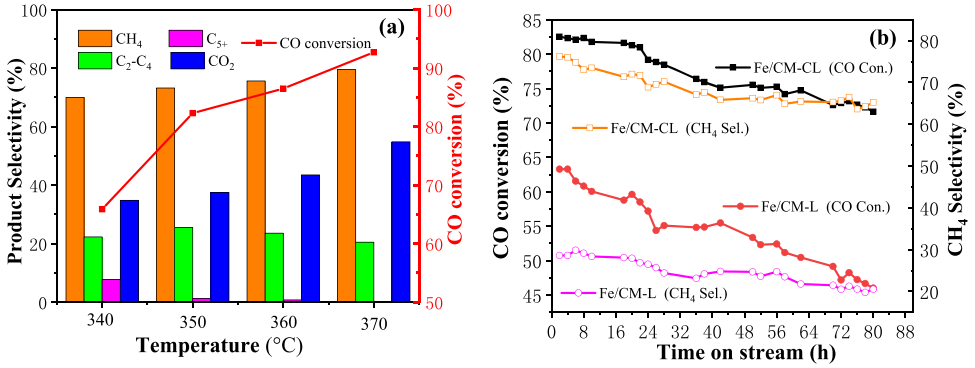

Figure 6. (a) CO conversion and selectivity of Fe/CM-CL with different temperatures, (b) conversions of CO and CH_4 selectivity with the time-on-stream on the catalysts Fe/CM-CL and Fe/CM-CL.

of peaks. The peaks at 707.9, 710.5, and 713.1 eV were attributed to the Fe^0 $2p_{3/2}$, Fe^{2+} $2p_{3/2}$, and Fe^{3+} $2p_{3/2}$ species, respectively. Additionally, the binding energies of the Fe^0 $2p_{1/2}$, Fe^{2+} $2p_{1/2}$ and Fe^{3+} $2p_{1/2}$ species were attributed to 720.8, 722.8, and 726.6 eV, respectively.[47] Most Fe elements in the Fe/CM-CL exhibit the oxidation valence state, which may be due to insufficient reduction at 600 °C or exposure to air and oxidation.

The results of the catalytic tests of FTS catalysts under conditions T = 350 °C, P = 2Mpa, and gas hourly space velocity (GHSV) = 8 $L{\cdot}h^{-1}{\cdot}g_{cat}^{-1}$ are further summarized in Table 1. It is evident from Table 1 that the iron particle size

https://doi.org/10.1021/acsomega.1c01935
ACS Omega 2021, 6, 16592−16599

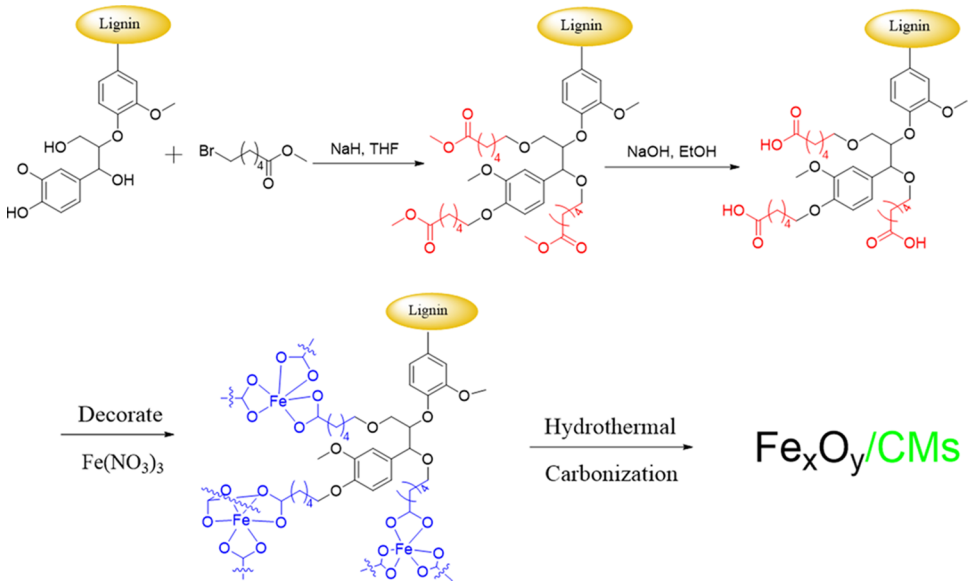

Figure 7. Synthetic route of lignin modification and Fe_xO_y/CMs.

shows significant effects on the trends of change of methane and lower olefin selectivity. With the iron particle size increase from 1.5−2 nm to 25−30 nm, the selectivity of lower olefins and C_{5+} increased from 15.9% and 1.3% for Fe/CM-CL to 33.6% and 12.7% for Fe/CM-L. However, the methane selectivity significantly decreased from 73.2% to 28.6% for Fe/CM-CL and Fe/CM-L. According to the results of N_2 adsorption and desorption analysis, it can be seen that the pore size of Fe/CM-L is larger than that of Fe/CM-CL. This inhibits the secondary hydrogenation reaction of lower olefins, which results in the selectivity of lower olefins increasing with the increase of the pore size. Furthermore, the supports with larger pore sizes are beneficial to the growth of carbon chains and are conducive to the formation of long-chain hydrocarbon C_{5+}.

The CO conversion and product distribution of Fe/CM-CL at different temperatures are shown in Figure 6(a). It can be seen from the figure that the conversion of carbon monoxide and the selectivity of methane show an upward trend with the increase in temperature. When the reaction temperature increases from 340 °C to 370 °C, the CO conversion and CH_4 selectivity increase by 26.8% and 9.6%, respectively. However, the selectivity of C_2-C_4 and C_{5+} decreased continuously. To make matters worse, the CO_2 content increased from 34.8% to 54.8%, and 20% of CO_2 increase comes from CO conversion. In other words, as the temperature increases, more CO will be converted to CO_2, not CH_4 or hydrocarbons. From the point of view of industrial applications, this is a noneconomical strategy because it consumes so much energy, in exchange for the increase of the greenhouse gas CO_2, rather than the target product. At the same time, very high reaction temperatures will cause the catalyst to agglomerate and even deactivate. Furthermore, in order to investigate the catalytic performance, the CO conversion and CH_4 selectivity of the Fe/CM-CL and Fe/CM-L, as a function of time-on-stream, are displayed in Figure 6(b) under conditions T = 350 °C, P = 2Mpa, and GHSV = 8 $L{\cdot}h^{-1}{\cdot}g_{cat}^{-1}$. It can be seen from Figure 6(b) that after 80 h of reaction, the CO conversion and CH_4 selectivity of the Fe/CM-L catalyst are 46.0% and 20.5%, respectively, which are 17.3.8% and 8.1% lower than the initial activity. In contrast, the stability of the Fe/CM-L catalyst is better, and its CO conversion and CH_4 selectivity are 71.6% and 65.2%, respectively.

In order to prove the superiority of Fe/CM-CL, the comparison of the merits of iron supported on carbon materials with some reported catalysts is shown in Table 1. It can be observed that under the same temperature and GHSV conditions, the CO conversion and CH_4 selectivity of the Fe/CM-CL catalyst with a smaller particle size are much higher than those of the 10Fe/hCNC catalyst. Further analysis shows that under the same temperature and particle size, with the increase in GHSV, the CO conversion and CH_4, C_{5+} selectivity decrease, while the C_2-C_4 selectivity increases. According to the literature,[21] the iron content has little effect on the conversion rate of CO and the selectivity of CH_4. Larger specific surface areas can absorb more syngas and improve the CO conversion rate.[48] Based on the above analysis, it can be observed that the CH_4 selectivity and CO conversion rate of Fe/CM-CL are better than those of these reported catalysts. The superior catalytic performance and higher methane selectivity are mainly attributed to the following factors: (1) The larger specific surface area and hierarchical porous structure can provide good adsorption, dissociation, reaction, and desorption channels for the catalytic reaction, as well as improve CO conversion;[48] (2) Nitrogen doping can increase the electron density on the iron surface, which is conducive to improving the catalytic activity; (3) The highly dispersed Fe nanoparticles can provide more active sites, which is beneficial to enhance catalytic activity;[19] (4) The smaller Fe nanoparticles are conducive to the enrichment of H on the surface, which is beneficial for the C atoms to react with H atoms to form methane, and it improves the selectivity of methane.[20,21]

3. CONCLUSIONS

In summary, we demonstrate an effective path to synthesize CL. By constructing the lignin−iron complex, small-sized iron supported on carbon materials was prepared, as a novel catalyst for FTS. The experimental results showed that the FTS activity

https://doi.org/10.1021/acsomega.1c01935
ACS Omega 2021, 6, 16592−16599

and selectivity are closely related to the particle size of iron; the smaller the iron particles, the more favorable the formation of methane is. Under the same reaction conditions, the methane selectivity of Fe/CM-CL (1.5−2.5 nm) achieves 73.2%, which is more than two times that of Fe/CM-CL (25−35 nm). Utilizing a lignin-based catalyst with a controllable metal size will promote the development of the pulp industry based on sustainable principles in energy-related applications.

4. EXPERIMENTAL SECTION

4.1. Chemicals and Materials. Lignin was acquired from Nanjing Forestry University. Sodium hydride, tetrahydrofuran (THF), ethanol, and ferric nitrate were acquired from Sinopharm Group Shanghai Chemical Reagent Co. Ltd. Methyl 4-bromopropionate and sodium hydride were acquired from Shanghai Aladdin Biochemical Technology Co. Ltd. For the synthesis gas H_2/CO/Ar, the volume ratio is 64/32/4, which was acquired from Changzhou Jinghua Industrial Gas Co. Ltd. All the chemicals were received without further purification.

4.2. Preparation of Fe/CM-CL and Fe/CM-L. Lignin (1 g) was dissolved in 60 mL of THF solution; after stirring for 30 min, 2.4 g of NaH was slowly added to the above solution in portions. Then, 2.6 mL of methyl 4-bromobutyrate was added to the reaction solution at room temperature for 12 h. Finally, the mixtures were added into the mixed solution of sodium hydroxide and ethanol (200 mL, V/V = 1:1) for reflux hydrolysis at 120 °C for 6 h in an oil bath. At the end of the reaction, organic solvents were removed using a rotary evaporator at 40 °C; then, the lignin solution was added to 500 mL of distilled water with continuous stirring overnight. The mixture was filtered using a 0.45 μm filter membrane, washed three times with distilled water, and dried using a freeze dryer. The obtained lignin was labeled as CL.

The Fe/CM-CL was synthesized using the two-step hydrothermal carbonization method. Following a typical preparation (Figure 7), 0.3 g of ferric nitrate and 0.5 g of CL were dissolved in 30 mL of distilled water (pH = 2.36) and then mixed and stirred for 30 min. After stirring, the mixed solution was transferred to a hydrothermal reactor at 180 °C for 24 h; then, the solution was centrifuged, washed, and dried, yielding the iron−lignin composite. Finally, carbonization was performed at 500 °C for 3 h at a heating rate of 1 °C/ min with argon protection. The obtained sample was recorded as Fe/CM-CL. Fe/CM-L was used as the control, and the reaction steps are the same as above, except using the unmodified lignin.

4.3. Characterization. Physical and chemical properties of the obtained materials were analyzed by XRD using a Rigaku D/Max2rB-II performed at 40 kV and 100 mA. The FT-IR functional group test was examined using a Fourier-transform infrared spectrometer (Nexus 470, USA). The binding energy was recorded by XPS (Perkin Elmer PHI5000C). All binding energy values were referenced to the C 1 s spectra of contaminant carbon at 284.6 eV. The microstructures of materials were observed by FE-SEM (Sigma 500), including element mapping and TEM (JEM-2100). N_2 adsorption−desorption isotherms were measured at −196 °C on an automated volumetric apparatus NOVA2000e (Quantachrome Instruments, USA).

The evaluation of catalysts was carried out in the self-assembled high-pressure fixed-bed microreactor, as shown in Figure 8. The detailed steps are similar to those in our previous work.[36] Typically, 0.3 g of the catalyst (50−60 mesh) was mixed well with an appropriate amount of quartz sand and then added to the reactor. Then, the catalyst was reduced with 10%H_2/AR at 450 °C for 8 h. After that, the syngas H_2/CO/N_2 (48/48/4) was passed over the catalyst bed at a flow rate of 40 mL/min (GHSV =8 L/hr./g_{cat}); the temperature was increased from room temperature to 350 °C, and the reaction pressure was adjusted to 2 MPa. Two gas chromatographs were used to detect the outlet gas online. N_2, H_2, CO, CO_2, and CH_4 were analyzed using the GC9860 gas chromatograph equipped with a thermal conductivity detector (TCD). The hydrocarbons (C_1-C_{30}) were tested using a PONA capillary column and a flame ionization detector (FID).

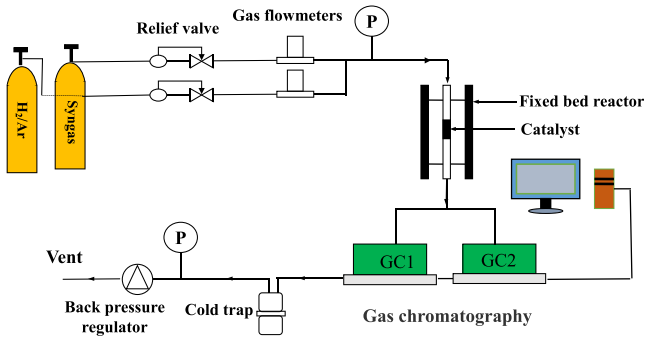

Figure 8. Scheme of the reaction system used for catalytic experiments.

AUTHOR INFORMATION

Corresponding Authors

Hengfei Qin − *School of Chemistry and Environmental Engineering and Jiangsu Key Laboratory of E-Waste Recycling, Jiangsu University of Technology, Changzhou City 213001, China*; orcid.org/0000-0001-7179-3907; Email: jlgqinhf@jsut.edu.cn

Quanfa Zhou − *Research Center of secondary Resources and Environment, Changzhou Institute of Technology, Changzhou City 213022, China*; Email: labzqf@czu.cn

Authors

Yan Li − *School of Chemistry and Environmental Engineering, Jiangsu University of Technology, Changzhou City 213001, China*

Ruoyu Dong − *School of Chemistry and Environmental Engineering, Jiangsu University of Technology, Changzhou City 213001, China*

Jiafeng Yuan − *School of Chemistry and Environmental Engineering, Jiangsu University of Technology, Changzhou City 213001, China*

Yue Zhou − *School of Chemistry and Environmental Engineering, Jiangsu University of Technology, Changzhou City 213001, China*

Yaxin Hu − *School of Chemistry and Environmental Engineering, Jiangsu University of Technology, Changzhou City 213001, China*

Hailang Jia − *School of Chemistry and Environmental Engineering, Jiangsu University of Technology, Changzhou City 213001, China*; orcid.org/0000-0001-8837-3802

Jirong Bai − *Research Center of secondary Resources and Environment, Changzhou Institute of Technology, Changzhou City 213022, China*

https://doi.org/10.1021/acsomega.1c01935
ACS Omega 2021, 6, 16592−16599

Jie Gong − *School of Chemistry and Environmental Engineering, Jiangsu University of Technology, Changzhou City 213001, China*

Jinlong Jiang − *Faculty of Chemical Engineering, Key Laboratory for Palygorskite Science and Applied Technology of Jiangsu Province, National & Local Joint Engineering Research Center for Deep Utilization Technology of Rock-salt Resource, Huaiyin Institute of Technology, Huaian 223003, P. R. China*

Complete contact information is available at: https://pubs.acs.org/10.1021/acsomega.1c01935

Notes

The authors declare no competing financial interest.

■ ACKNOWLEDGMENTS

This work was supported by the National Natural Science Foundation of China (Grant No. 31800495), Natural Science Foundation of Jiangsu Province (BK20181040), China Postdoctoral Science Foundation (2019 M653654), National key research and development project (Grant No. 2018YFC1902503-2), the College Students' Training Program of Innovation and Entrepreneurship of Jiangsu Province (201911463011Z) of China. We are grateful for the financial support from the Opening Topic of National & Local Joint Engineering Research Center for Deep Utilization Technology of Rock-Salt Resource (SF201804).

■ REFERENCES

(1) Galvis, H. M. T.; Bitter, J. H.; Khare, C. B.; Ruitenbeek, M.; Dugulan, A. I.; de Jong, K. P. Supported Iron Nanoparticles as Catalysts for Sustainable Production of Lower Olefins. *Science* **2012**, *335*, 835−838.

(2) Chen, W.; Fan, Z. L.; Pan, X. L.; Bao, X. H. Effect of confinement in carbon nanotubes on the activity of Fischer-Tropsch iron catalyst. *J. Am. Chem. Soc.* **2008**, *130*, 9414−9419.

(3) Cheng, Y.; Lin, J.; Xu, K.; Wang, H.; Yao, X. Y.; Pei, Y.; Yan, S. R.; Qiao, M. H.; Zong, B. N. Fischer-Tropsch Synthesis to Lower Olefins over Potassium-Promoted Reduced Graphene Oxide Supported Iron Catalysts. *ACS Catal.* **2016**, *6*, 389−399.

(4) Qin, H. F.; Wang, B.; Zhang, C. Y.; Zhu, B. L.; Zhou, Y.; Zhou, Q. F. Lignin based synthesis of graphitic carbon-encapsulated iron nanoparticles as effective catalyst for forming lower olefins via Fischer-Tropsch synthesis. *Catal. Commun.* **2017**, *96*, 28−31.

(5) Zhong, M.; Wang, J. G.; Chen, C. B.; Ma, Z. C.; Jia, L. T.; Hou, B.; Li, D. B. Incorporating silicon carbide nanoparticles into Al_2O_3@Al to achieve an efficient support for Co-based catalysts to boost their catalytic performance towards Fischer-Tropsch synthesis. *Catal. Sci. Technol.* **2019**, *9*, 6037−6046.

(6) Tsakoumis, N. E.; Patanou, E.; Logdberg, S.; Johnsen, R. E.; Myrstad, R.; van Beek, W.; Rytter, E.; Blekkan, E. A. Structure-Performance Relationships on Co-Based Fischer-Tropsch Synthesis Catalysts: The More Defect-Free, the Better. *ACS Catal.* **2019**, *9*, 511−520.

(7) Nohtani, R.; Mirzaei, A. A.; Eshraghi, A. Synthesis of Fe-Co-Ce/Zeolite A-3 Catalysts and their Selectivity to Light Olefins for Fischer-Tropsch Synthesis in Fixed-Bed Reactor. *Catal. Lett.* **2019**, *149*, 522−532.

(8) Chen, Y.; Li, X.; Nisa, M. U.; Lv, J.; Li, Z. H. ZIF-67 as precursor to prepare high loading and dispersion catalysts for Fischer-Tropsch synthesis: Particle size effect. *Fuel* **2019**, *241*, 802−812.

(9) Azizi, H. R.; Mirzaei, A. A.; Sarani, R.; Kaykhaii, M. Pilot scale study of Co-Fe-Ni nanocatalyst for CO hydrogenation in Fischer-Tropsch synthesis. *Iran J Catal* **2019**, *9*, 223−231.

(10) Liu, C. C.; He, Y.; Wei, L.; Zhang, Y. H.; Zhao, Y. X.; Hong, J. P.; Chen, S. F.; Wang, L.; Li, J. L. Hydrothermal Carbon-Coated TiO_2 as Support for Co-Based Catalyst in Fischer-Tropsch Synthesis. *ACS Catal.* **2018**, *8*, 1591−1600.

(11) Jiang, Z. S.; Zhao, Y. H.; Huang, C. F.; Song, Y. H.; Li, D. P.; Liu, Z. T.; Liu, Z. W. Metal-support interactions regulated via carbon coating - A case study of Co/SiO_2 for Fischer-Tropsch synthesis. *Fuel* **2018**, *226*, 213−220.

(12) Qin, H. F.; Jian, R. H.; Bai, J. R.; Tang, J. H.; Zhou, Y.; Zhu, B. L.; Zhao, D. J.; Ni, Z. J.; Wang, L. B.; Liu, W. Q.; Zhou, Q. F.; Li, X. Influence of Molecular Weight on Structure and Catalytic Characteristics of Ordered Mesoporous Carbon Derived from Lignin. *ACS Omega* **2018**, *3*, 1350−1356.

(13) Hong, G. H.; Noh, Y. S.; Park, J. I.; Shin, S. A.; Moon, D. J. Effect of catalytic reactor bed dilution on product distribution for Fischer-Tropsch synthesis over $Ru/Co/Al_2O_3$ catalyst. *Catal. Today* **2018**, *303*, 136−142.

(14) Long, J. L.; Shen, K.; Li, Y. W. Bifunctional N-Doped Co@C Catalysts for Base-Free Transfer Hydrogenations of Nitriles: Controllable Selectivity to Primary Amines vs Imines. *ACS Catal.* **2017**, *7*, 275−284.

(15) Hatami, B.; Asghari, A.; Tavasoli, A.; Zamani, Y.; Zamaniyan, A. Effects of Functionalization of Carbon Nanotubes on Activity and Selectivity of Co/CNT Catalysts in Fischer-Tropsch Synthesis. *Phys Chem Res* **2018**, *6*, 795−804.

(16) Xiong, H. F.; Motchelaho, M. A.; Moyo, M.; Jewell, L. L.; Coville, N. J. Effect of Group I alkali metal promoters on Fe/CNT catalysts in Fischer-Tropsch synthesis. *Fuel* **2015**, *150*, 687−696.

(17) Qin, H. F.; Kang, S. F.; Wang, Y. G.; Liu, H.; Ni, Z. J.; Huang, Y. K.; Li, Y. G.; Li, X. Lignin-Based Fabrication of Co@C Core-Shell Nanoparticles as Efficient Catalyst for Selective Fischer-Tropsch Synthesis of C_{5+} Compounds. *ACS Sustainable Chem. Eng.* **2016**, *4*, 1240−1247.

(18) Liu, R. J.; Xu, Y.; Li, Z. H.; Ma, X. B. A Facile and Efficient Modification of CNTs for Improved Fischer-Tropsch Performance on Iron Catalyst: Alkali Modification. *ChemCatChem* **2016**, *8*, 1454−1458.

(19) Liu, J. X.; Wang, P.; Xu, W.; Hensen, E. J. M. Particle Size and Crystal Phase Effects in Fischer-Tropsch Catalysts. *Engineering* **2017**, *3*, 467−476.

(20) Galvis, H. M. T.; Bitter, J. H.; Davidian, T.; Ruitenbeek, M.; Dugulan, A. I.; de Jong, K. P. Iron Particle Size Effects for Direct Production of Lower Olefins from Synthesis Gas. *J. Am. Chem. Soc.* **2012**, *134*, 16207−16215.

(21) Xie, J.; Yang, J.; Dugulan, A. I.; Holmen, A.; Chen, D.; de Jong, K. P.; Louwerse, M. J. Size and Promoter Effects in Supported Iron Fischer-Tropsch Catalysts: Insights from Experiment and Theory. *ACS Catal.* **2016**, *6*, 3147−3157.

(22) Sheng, Z. M.; Wang, J. N. Thin-walled carbon nanocages: Direct growth, characterization, and applications. *Adv. Mater.* **2008**, *20*, 1071−1075.

(23) Miao, J. Y.; Hwang, D. W.; Narasimhulu, K. V.; Lin, P. I.; Chen, Y. T.; Lin, S. H.; Hwang, L. P. Synthesis and properties of carbon nanospheres grown by CVD using Kaolin supported transition metal catalysts. *Carbon* **2004**, *42*, 813−822.

(24) Erokhin, A. V.; Lokteva, E. S.; Yermakov, A. Y.; Boukhvalov, D. W.; Maslakov, K. I.; Golubina, E. V.; Uimin, M. A. Phenylacetylene hydrogenation on Fe@C and Ni@C core-shell nanoparticles: About intrinsic activity of graphene-like carbon layer in H-2 activation. *Carbon* **2014**, *74*, 291−301.

(25) Paraskevas, L.; Caps, V.; Tsang, S. C. Syntheses of carbon encapsulated magnetic FeNi nanoparticle via decompositions of methane and benzene. *Carbon* **2006**, *44*, 820−823.

(26) Qin, H. F.; Kang, S. F.; Huang, Y. K.; Liu, S. Y.; Fang, Y.; Li, X.; Wang, Y. G. Lignin based synthesis of carbon nanocages assembled from graphitic layers with hierarchical pore structure. *Mater. Lett.* **2015**, *159*, 463−465.

(27) Bi, R.; Lawoko, M.; Henriksson, G. Phoma herbarum, a soil fungus able to grow on natural lignin and synthetic lignin (DHP) as sole carbon source and cause lignin degradation. *J Ind Microbiol Biot* **2016**, *43*, 1175−1182.

(28) Wu, J.; Chandra, R.; Saddler, J. Alkali-oxygen treatment prior to the mechanical pulping of hardwood enhances enzymatic hydrolysis and carbohydrate recovery through selective lignin modification. *Sustain Energ Fuels* **2019**, *3*, 227−236.
(29) Takada, M.; Chandra, R.; Wu, J.; Saddler, J. N. The influence of lignin on the effectiveness of using a chemithermomechanical pulping based process to pretreat softwood chips and pellets prior to enzymatic hydrolysis. *Bioresour. Technol.* **2020**, *302*, No. 122895.
(30) Liu, Y. Z.; Guo, B. T.; Xia, Q. Q.; Meng, J.; Chen, W. S.; Liu, S. X.; Wang, Q. W.; Liu, Y. X.; Li, J.; Yu, H. P. Efficient Cleavage of Strong Hydrogen Bonds in Cotton by Deep Eutectic Solvents and Facile Fabrication of Cellulose Nanocrystals in High Yields. *ACS Sustainable Chem. Eng.* **2017**, *5*, 7623−7631.
(31) Liu, L. Y.; Hua, Q.; Renneckar, S. A simple route to synthesize esterified lignin derivatives. *Green Chem.* **2019**, *21*, 3682−3692.
(32) Liu, L. Y.; Cho, M.; Sathitsuksanoh, N.; Chowdhury, S.; Renneckar, S. Uniform Chemical Functionality of Technical Lignin Using Ethylene Carbonate for Hydroxyethylation and Subsequent Greener Esterification. *ACS Sustainable Chem. Eng.* **2018**, *6*, 12251−12260.
(33) Xiong, F. Q.; Han, Y. M.; Wang, S. Q.; Li, G. Y.; Qin, T. F.; Chen, Y.; Chu, F. X. Preparation and Formation Mechanism of Renewable Lignin Hollow Nanospheres with a Single Hole by Self-Assembly. *ACS Sustainable Chem. Eng.* **2017**, *5*, 2273−2281.
(34) Li, Y. L.; Wu, M.; Wang, B.; Wu, Y. Y.; Ma, M. G.; Zhang, X. M. Synthesis of Magnetic Lignin-Based Hollow Microspheres: A Highly Adsorptive and Reusable Adsorbent Derived from Renewable Resources. *ACS Sustainable Chem. Eng.* **2016**, *4*, 5523−5532.
(35) Ma, Y. L.; Dai, J. X.; Wu, L. L.; Fang, G. Z.; Guo, Z. H. Enhanced anti-ultraviolet, anti-fouling and anti-bacterial polyelectrolyte membrane of polystyrene grafted with trimethyl quaternary ammonium salt modified lignin. *Polymer* **2017**, *114*, 113−121.
(36) Qin, H. F.; Zhou, Y.; Bai, J. R.; Zhu, B. L.; Ni, Z. J.; Wang, L. B. A.; Liu, W. G.; Zhou, Q. F.; Li, X. Lignin-Derived Thin-Walled Graphitic Carbon-Encapsulated Iron Nanoparticles: Growth, Characterization, and Applications. *ACS Sustainable Chem. Eng.* **2017**, *5*, 1917−1923.
(37) Ying, W. J.; Shi, Z. J.; Yang, H. Y.; Xu, G. F.; Zheng, Z. F.; Yang, J. Effect of alkaline lignin modification on cellulase-lignin interactions and enzymatic saccharification yield. *Biotechnol Biofuels* **2018**, *11*, 214.
(38) Cherif, M. F.; Trache, D.; Brosse, N.; Benaliouche, F.; Tarchoun, A. F. Comparison of the Physicochemical Properties and Thermal Stability of Organosolvent and Kraft Lignins from Hardwood and Softwood Biomass for Their Potential Valorization. *Waste Biomass Valori* **2020**.
(39) Luo, S. P.; Gao, L.; Guo, W. J., Effect of incorporation of lignin as bio-polyol on the performance of rigid lightweight wood-polyurethane composite foams. *J Wood Sci.* **2020**, *66*, (), DOI: 10.1186/s10086-020-01872-5.
(40) Wu, K.; Ying, W. J.; Shi, Z. J.; Yang, H. Y.; Zheng, Z. F.; Zhang, J. Y.; Yang, J. Fenton Reaction-Oxidized Bamboo Lignin Surface and Structural Modification to Reduce Nonproductive Cellulase Binding and Improve Enzyme Digestion of Cellulose. *ACS Sustainable Chem. Eng.* **2018**, *6*, 3853−3861.
(41) Figureueiredo, P.; Ferro, C.; Kemell, M.; Liu, Z. H.; Kiriazis, A.; Lintinen, K.; Florindo, H. F.; Yli-Kauhaluoma, J.; Hirvonen, J.; Kostiainen, M. A.; Santos, H. A. Functionalization of carboxylated lignin nanoparticles for targeted and pH-responsive delivery of anticancer drugs. *Nanomedicine-Uk* **2017**, *12*, 2581−2596.
(42) Thommes, M.; Kaneko, K.; Neimark, A. V.; Olivier, J. P.; Rodriguez-Reinoso, F.; Rouquerol, J.; Sing, K. S. W. Physisorption of gases, with special reference to the evaluation of surface area and pore size distribution (IUPAC Technical Report). *Pure Appl. Chem.* **2015**, *87*, 1051−1069.
(43) Ramasubbu, V.; Kumar, P. R.; Mothi, E. M.; Karuppasamy, K.; Kim, H. S.; Maiyalagan, T.; Shajan, X. S. Highly interconnected porous TiO2-Ni-MOF composite aerogel photoanodes for high power conversion efficiency in quasi-solid dye-sensitized solar cells. *Appl. Surf. Sci.* **2019**, *496*, No. 143646.
(44) Wan, W. C.; Wei, S. Q.; Li, J. G.; Triana, C. A.; Zhou, Y.; Patzke, G. R. Transition metal electrocatalysts encapsulated into N-doped carbon nanotubes on reduced graphene oxide nanosheets: efficient water splitting through synergistic effects. *J. Mater. Chem. A* **2019**, *7*, 15145−15155.
(45) Wang, K.; Chen, H. X.; Zhang, X. F.; Tong, Y. X.; Song, S. Q.; Tsiakaras, P.; Wang, Y. Iron oxide@graphitic carbon core-shell nanoparticles embedded in ordered mesoporous N-doped carbon matrix as an efficient cathode catalyst for PEMFC. *Appl Catal B-Environ* **2020**, *264*, No. 118468.
(46) Li, F. Y.; Li, H.; Liu, X. X.; Wang, L. B.; Lu, Y.; Hu, X. L. Scalable Synthesis of Fe/N-Doped Porous Carbon Nanotube Frameworks for Aqueous Zn-Air Batteries. *Chem-Eur J* **2019**, *25*, 635−641.
(47) Chen, Y. F.; Li, Z. J.; Zhu, Y. B.; Sun, D. M.; Liu, X. E.; Xu, L.; Tang, Y. W. Atomic Fe Dispersed on N-Doped Carbon Hollow Nanospheres for High-Efficiency Electrocatalytic Oxygen Reduction. *Adv. Mater.* **2019**, *31* ().
(48) Liu, Y.; Chen, J. F.; Zhang, Y. The effect of pore size or iron particle size on the formation of light olefins in Fischer-Tropsch synthesis. *RSC Adv.* **2015**, *5*, 29002−29007.
(49) Zhuo, O.; Yang, L. J.; Gao, F. J.; Xu, B. L.; Wu, Q.; Fan, Y. N.; Zhang, Y.; Jiang, Y. F.; Huang, R. S.; Wang, X. Z.; Hu, Z. Stabilizing the active phase of iron-based Fischer-Tropsch catalysts for lower olefins: mechanism and strategy. *Chem. Sci.* **2019**, *10*, 6083−6090.

https://doi.org/10.1021/acsomega.1c01935
ACS Omega 2021, 6, 16592−16599